Chemical Engineering Journal Advances 12 (2022) 100365

Contents lists available at ScienceDirect

Chemical Engineering Journal Advances

journal homepage: www.sciencedirect.com/journal/chemical-engineering-journal-advances

Comparative study of two non-Newtonian fluids with bioconvective induced MHD flow in presence of multiple slips, heat source/sink and nonlinear thermal radiation

Anil Kumar Gautam [a], Sohita Rajput [a], Krishnendu Bhattacharyya [a,*], Amit Kumar Pandey [a], Ali J. Chamkha [b], Momtaz Begum [c]

[a] Department of Mathematics, Institute of Science, Banaras Hindu University, Varanasi-221005, Uttar Pradesh, India
[b] Faculty of Engineering, Kuwait College of Science and Technology, Doha District, Kuwait
[c] Department of Computer science and Engineering, Prime University, Mirpur-1, Dhaka, Bangladesh

ARTICLE INFO

Keywords:
Bioconvection
Non-Newtonian fluids
Induced MHD flow
Multiple slips
Heat source/sink
Nonlinear thermal radiation

ABSTRACT

The present manuscript deals with bioconvective induced magnetohydrodynamic (MHD) flow of non-Newtonian fluids with simultaneous effects of multiple slips, heat source/sink, and nonlinear thermal radiation. Flows of Maxwell and Casson fluids are considered separately, but a single governing momentum conservation equation is constructed by combining these two flow models. Transformed governing equations are solved by MATLAB solver 'bvp4c'. The objective of the current study is to check the comparative behaviour of two non-Newtonian fluids viz., Maxwell and Casson in presence of induced MHD effect with the bioconvective phenomenon and slip effect. The main findings reveal the growth of velocity and fall of microorganisms' motile density with induced magnetic number. With higher values of Peclet number and microorganism concentration difference parameter, the microbe's motile density significantly reduces. The temperature hike is witnessed with heat generation/absorption, thermal radiation, and temperature ratio parameters. Also, for a fixed set of values of parameters the Casson fluid velocity is more prominent than the Maxwell fluid velocity and the scenario is the opposite for the motile density of microorganisms. Velocity increases, whereas motile density decreases with raising the amount of magnetic Prandtl number. Casson fluids have more velocity than Maxwell fluids, whereas the movement of the motile density of microorganisms is showing prominency for Maxwell fluids. The magnitude of surface drag and surface cooling rate are at a higher level for Casson fluid in comparison with Maxwell fluid. The motile density number enhances with the microorganism concentration difference parameter and Peclet number.

1. Introduction

Many fluid materials used in modern-day engineering have flow characteristics, which are not explained by the fluid model obeying Newton's viscosity law. So, non-Newtonian fluids become indispensable. Non-Newtonian fluid flow has recently gained strong fame to address significant issues in many sectors of industry, science, and commerce. Non-Newtonian fluids are necessarily contained viscosity, i.e., in another word, we can say that they have viscous properties. Beyond this, some industrial non-Newtonian fluids have viscous properties as well as elastic properties and the constitutive equations for those include yield shear stress. Due to this reason, these fluid models are most effective for low-molecular-weight polymers.

In fluid dynamics as well as in the engineering sector and commercial sector, heat and mass transports inside different non-Newtonian fluids models having several physical properties are really important. The real instances of non-Newtonian fluid flows are visible in molten polymers, volcanic lava, some certified paints, drilling mud, cosmetics, oils, polycrystalline melts, liquid suspensions, materials used for food production, and many others. Maxwell fluid is a non-Newtonian fluid type, which was proposed by Maxwell [1]. The concept of stress relaxation is explained by using the Maxwell model, which also includes the effect of shear-dependent viscosity. Hayat and Qasim [2] introduced Maxwell fluid flow with thermophoresis and Joule heating. Whereas, the flow of Maxwell fluid inside a porous channel was studied by Hayat et al. [3]. Shateyi [4] presented the same flow across an expanding sheet with a chemical reaction. While Mukhopadhyay [5] investigated the unsteady

* Corresponding author.
E-mail address: krish.math@yahoo.com (K. Bhattacharyya).

https://doi.org/10.1016/j.ceja.2022.100365
Received 20 April 2022; Received in revised form 4 July 2022; Accepted 13 July 2022
Available online 16 July 2022

Nomenclature

a	Stretching rate
b	Chemotaxis coefficient
Bh	Local microorganism density number
C	Concentration
C_w	Concentration at the surface
C_∞	Ambient fluid concentration
C_β	Casson fluid parameter
c_p	Specific heat
D_s	Microorganism diffusion coefficient
f	Dimensionless stream function
f'	Dimensionless velocity
Gr_T, Gr_C, Gr_s	Thermal, solutal and microorganism Grashof numbers
g, g'	Dimensionless magnetic induction components
g^*	Gravitation acceleration
h	Magnetic stream function
k^*	Mean absorption coefficient
Lb	Bioconvection Lewis number
Le	Lewis number
L_1, L_2, L_3, L_4	Velocity, temperature, concentration and microorganism slip lengths
M^*	Induced magnetic number
M_m	Maxwell fluid parameter
Nu	Local Nusselt number
Nr	Radiation parameter
Pe	Peclet number
Pr	Prandtl number
Q_0	Heat generation/absorption parameter
q_h	Heat flux at the wall
q_n	Microorganism flux
q_s	Mass flux
R	Reaction rate constant
Re_x	Reynolds number
s	Microorganisms field
s_w	Microorganism at the surface
s_∞	Ambient fluid microorganism
Sc	Schmidt number
Sh	Local Sherwood number
T	Fluid Temperature
T_w	Temperature at the surface
T_∞	Ambient fluid temperature
U_w	Stretching velocity
(u, v)	Velocity component along x-axis and y-axis, respectively
(x, y)	Space coordinates
W_c	Cell moving speed

Greek symbols

α_e	Magnetic diffusivity
α_1	Thermal diffusivity
$\beta_T, \beta_C, \beta_s$	Volumetric coefficients of thermal, solutal and motile density expansions
ε	Magnetic Prandtl number
η	Dimensionless variable
θ	Temperature distribution
λ, δ, γ	Thermal, solutal and microorganism buoyancy parameters
$\lambda_1, \lambda_2, \lambda_3$	Velocity, thermal, solutal and motile microorganism density slip parameters
λ_m	Deborah number
μ	Dynamic viscosity
μ_h	Magnetic permeability
σ^*	Stefan-Boltzmann constant
φ	Volumetric concentration
χ	Microorganism concentration
ψ	Stream function
Ω	Microorganisms' concentration difference parameter

state of Maxwell flow on the stretched wall with a heat source/sink. Maxwell fluid also has many industrial usages, such as, in application of paints in polymer processing industry and the movement of biological fluids. Another type of non-Newtonian fluid that grabs the researcher's interest is named Casson fluid [6] (e.g., tomato sauce, human blood, jelly, and honey). Some of the potential uses of Casson liquid are in penetrating procedures, in various bio-engineering processes, in the wide domain of material science with engineering phenomena, and also in many nutrition procedures. Some essential features of Casson fluid flows were described by Fredrickson [7] and Mernone et al. [8].

The characters of boundary layer flow past a stretching sheet are highlighted due to its applications in the field of engineering. Many articles on the boundary layer flow past a stretching sheet may be found in the literature [9–11]. Later, Hamad [12] proposed an analytic solution for the flow over stretching sheet in presence of nanoparticles. Casson fluid flow over stretching sheet involving in the heat transfer process along with other flow properties is very important for many industrial operations [13–17]. On the other hand, the correlation of different non-Newtonian fluid models explores various important features and their applicability in many physical flow situations. In this context, Boyd et al. [18] discussed the comparative behaviour of the Casson and Carreau-Yasuda model. Kumar et al. [19] and Kumaran et al. [20] successfully integrated heat sink/source, cross-diffusion, and chemical reaction into an analysis of hydromagnetic flow of Maxwell and Casson nanofluids across the extended surfaces. Recently, Shah et al. [21] proposed the comparison of Maxwell and Casson fluids through an extending surface.

In the above-described flows, the standard no-slip condition at the solid barrier is a typical component in the analysis, i.e., the relative velocity between the fluid and the solid is zero. However, there are some flow situations when this criterion does not apply. Navier [22] presented a broader boundary condition that takes into consideration of the possibility of the fluid slipping on a solid surface. The slip boundary condition was also discussed by Maxwell [23] using the kinetic theory of gases. Andersson [24] introduced this slip condition in boundary-layer flow on a stretched surface. The slip effects on chemically reactive solute diffusion on a porous vertical stretching sheet were given by Bhattacharyya and Layek [25]. Recently, Bhatti et al. [26] designed a computational framework for stagnation nanoflow flow past a stretching surface with the control of velocity slip and thermal slip effect.

The heat transfer phenomenon which is much impacted by thermal radiation has huge applications in industry and technology-related processes, such as nuclear power, gas turbine plants, and various propulsion devices. Khan et al. [27] reported the influence of radiative heat flux and chemical reaction of Carreau-Yasuda flow and found the rate of entropy-optimization. In the context of radiative slip flow, Mukhopadhyay and Gorla [28] investigated the flow on porous exponentially stretched sheets with thermal radiation and partial slip.

An unrefined experienced which is fundamentally related to the self-propelled microorganism's suspension is fame as bioconvection. Bioconvection is a phenomenon that occurs when bacteria or biological solutions are combined with fluid. This behaviour is most commonly observed in diluted fluids, when bacteria tend to travel, resulting in the production of instability owing to density. Bioconvection has numerous applications in the theory of biological science, and the research involving the area of bio-micro-systems. Additionally, one probable application of the concept of bioconvection is in the rehabilitation of microbial-enhanced oil to enhance its immunity via injecting the

microorganisms as well as nutrients, like vitamin, protein, fiber, etc., into the layers of oil-bearing for correcting the differences in the level of ability of substances to allow gases or liquids to pass through it. Due to this reason, understanding the mechanism of bioconvection with other physical aspects is very important. Furthermore, when the property of non-Newtonian fluids is involved in such a phenomenon, then physical models are more applicable and interesting. The other physical aspects, like the involvement of nonlinear thermal radiation, multiple slips, and induced magnetic field are set for making the physical model more realistic. Chu et al. [29] investigated Maxwell nanofluid flow with gyrotactic microorganisms, nonlinear radiative effect, and heat generation. In the presence of motile bacteria, Ramzan et al. [30] illustrated radiative magnetized nanofluid flow with microorganisms and chemical reaction. The inclusion of partial slip in the bioconvective flow of Cross nanofluids across moving wedges was explained by Alshomrani et al. [31]. Whereas, Khan et al. [32] investigated MHD Maxwell fluid flow with gyrotactic microorganisms. Ramesh et al. [33] explained Maxwell nanofluid flow with bioconvection, activation energy and nonlinear thermal radiation. The Cattaneo-Christov analysis in the context of Maxwell nanofluid and bioconvection was done by Chu et al. [34]. Shahid et al. [35] discussed the application of Carreau nanoliquid in solar energy with Arrhenius activation energy and bioconvection taken into account. To realize the thermal behaviour for the significance of thermal application, Al-Khaled and Khan [36] found an approximate solution of Casson nanofluid with consideration of gyrotactic microorganisms and activation energy. The analysis of Eyring-Powell liquid with bioconvection phenomenon for the unsteady case was studied by Khan and Ali [37]. The thixotropic nanoliquid with bioconvection implication for the Riga surface was discussed by Khan et al. [38]. Some important features of bioconvection in the context of Jeffrey nanoliquid for modified Prandtl number with were reported by Khan and Tlili [39]. MHD nanofluid flow of Williamson fluid with bioconvection effect for rotating circular plate was initiated and fully explained by Bhatti et al. [40] through DTM-pade approach. Koriko et al. [41] found the outcomes of correlation of bioconvection and nanofluid in MHD flow for thixotropic fluid. The implications of gyrotactic bioconvection and activation energy for cross nanofluid was discussed numerically by Shi et al. [42].

In thermal energy science, a situation, when high-temperature differences are found between the surface and ambient fluid, then at this situation, the concept of heat source/sink is used. Due to the wide range of heat source/sink applications in energy conservation systems, it is necessary to study the control of the heat source/sink phenomenon in engineering problems in modern-day requirements. In the progress of study related with the occurrence of heat source/sink, Chu et al. [43] found the outcomes of the effect of heat source/sink, with radiative flux. Simultaneous behaviour of nonlinear thermal radiation and heat generation effect on the flow of micropolar nanofluid was discussed by Pattanaik et al. [44]. Some other important studies are found considering different physical aspects along with heat source/sink in literature [45–48].

One of the major areas of fluid mechanics which take more attention from researchers is magnetohydrodynamics, which describes the motion of electrically conducting fluids. Various flow characteristics were examined by many expert scientists assuming magnetic field effect. Magnetic field impact on viscous flow is relevant in a variety of industrial processes, including MHD electrical power generation, crude oil purification, magnetic materials processing, etc. In the progress of different physical models for the MHD effect, Shah et al. [49] investigated the MHD effect for free convection over the vertical plate. In addition, Shah et al. [50] also studied the impact of MHD flow in a cylindrical tube. In addition, Chu et al. [51] explained heat and mass transfer analysis of dual nature for stagnation point flow of Carreau nanoliquid with magnetic effect. Nazeer [52] analyzed the approximate analytic solution of MHD flow in a microchannel for second-grade fluid. Magnetic lines of forces are used to characterize the induced magnetic field. Many scholars are interested in studying the effect of induced magnetic fields on boundary layer flow as MHD flows and heat transfer have a wide application in many industrial processes when an induced magnetic field is implemented. Ibrahim [53] investigated the influence of induced magnetic field on MHD stagnation-point flow in presence of nanoparticles.

There are several applications of induced MHD flow with bioconvection in various fields, i.e., engineering, medical, and bio-fuel applications. Due to this reason, researchers are interested to work in the field of bioconvection in presence of magnetic effect. In the recent context to the area of Rheology, many researchers focus their attention on bio-convection with considering non-Newtonian fluids because it is more realistic and applicable. Motivated by the wide implications of bioconvection and the impact of induced magnetic field on the flow of non-Newtonian fluids, the challenge of correlating Maxwell and Casson fluid flows with bio-convection and induced magnetic field in presence of multiple slips, heat source/sink, and non-linear thermal radiation has been undertaken in this investigation. The additional motivation behind the present study is the noteworthy results which are found in the above-cited literature in the context of bioconvection MHD flow of non-Newtonian fluid. Also, there is no such study which discusses the comparison between two non-Newtonian fluids in the presence of nonlinear thermal radiation, heat source/sink, and multiple slips with an induced magnetic field. Also, the inclusions of bio-convection and induced magnetic field in presence of multiple slips and thermal radiation are making the problem more interesting and attractive from the viewpoints of several engineering applications. The MATLAB solver ‘bvp4c’ effectively provides numerical solutions to transformed governing equations, i.e., non-linear ordinary differential equations (ODEs). The generated results are exhibited and explained through graphical and tabular presentations. The novelty of the present analysis is inside the theoretical as well as numerical comparison of the behaviour of two non-Newtonian fluids with some applicable phenomena, such as the impact of bioconvection, non-linear structure of thermal radiation, and multiple slip effects in the presence of induced magnetic field and heat generation/absorption.

2. Basic governing equations

This comprehensive work incorporates bio-convection of self-motivated microorganisms, multiple slips, and non-linear thermal radiation in induced MHD flow of Maxwell and Casson fluids. Fluid flow is laminar, two-dimensional and incompressible. The magnetic Reynolds number is high to consider the effect of an induced magnetic field. The flow generated by the linear stretching sheet is a boundary layer flow. Also, the model is developed with the assumption of steady-state flow. The velocity of the expansion of sheet is $U_w = ax$, with $a(> 0)$ being a constant and the dimension of $a(> 0)$ is $[T^{-1}]$. Considering all the aforesaid assumptions, the governing boundary layer equations of motion are specified as [54,55]:

$$\frac{\partial u}{\partial x}+\frac{\partial v}{\partial y}=0, \tag{1}$$

$$\frac{\partial H_1}{\partial x}+\frac{\partial H_2}{\partial y}=0, \tag{2}$$

$$u\frac{\partial u}{\partial x}+v\frac{\partial u}{\partial y}=\upsilon\left(1+\frac{1}{C_\beta}\right)\left(\frac{\partial^2 u}{\partial y^2}\right)-\lambda_M\left(u^2\frac{\partial^2 u}{\partial x^2}+2uv\frac{\partial^2 u}{\partial x\partial y}+v^2\frac{\partial^2 u}{\partial y^2}\right)$$

$$+\frac{\mu_h}{4\pi\rho}\left[H_1\frac{\partial H_1}{\partial x}+H_2\frac{\partial H_1}{\partial y}\right]+g^*\beta_T(T-T_\infty)+g^*\beta_C(C-C_\infty)+g^*\beta_s(s-s_\infty), \tag{3}$$

$$u\frac{\partial H_1}{\partial x}+v\frac{\partial H_1}{\partial y}=H_1\frac{\partial u}{\partial x}+H_2\frac{\partial u}{\partial y}+\alpha_e\frac{\partial^2 H_1}{\partial y^2}, \tag{4}$$

$$u\frac{\partial T}{\partial x}+v\frac{\partial T}{\partial y}=\alpha_1\frac{\partial^2 T}{\partial y^2}-\frac{1}{\rho c_p}\frac{\partial q_r}{\partial y}+\frac{Q}{\rho c_p}(T-T_\infty), \tag{5}$$

$$u\frac{\partial C}{\partial x}+v\frac{\partial C}{\partial y}=D_m\frac{\partial^2 C}{\partial y^2}-R(C-C_\infty), \tag{6}$$

$$u\frac{\partial s}{\partial x}+v\frac{\partial s}{\partial y}+\frac{bW_c}{(C_w-C_\infty)}\left[\frac{\partial}{\partial y}\left(s\frac{\partial C}{\partial y}\right)\right]=D_s\left(\frac{\partial^2 s}{\partial y^2}\right), \tag{7}$$

with boundary conditions

$$\left.\begin{aligned} &u=U_w+L_1\frac{\partial u}{\partial y},\ v=0,\ \frac{\partial H_1}{\partial y}=H_2=0,\\ &T=T_w+L_2\frac{\partial T}{\partial y},\ C=C_w+L_3\frac{\partial C}{\partial y},\ s=s_w+L_4\frac{\partial s}{\partial y}, \end{aligned}\right\}\ \text{at } y=0, \tag{8}$$

$$\left.\begin{aligned} &u\to 0,\ T\to T_\infty,\ C\to C_\infty,\\ &s\to s_\infty,\ H_1\to H_e(x)=H_0x \end{aligned}\right\}\ \text{as } y\to\infty. \tag{9}$$

In the above equations, Eq. (1) and Eq. (2) are continuity and its corresponding induced magnetic field equations, respectively. Eqs. (3) and (4) represent the momentum and its associated induced magnetic field equations. The heat, concentration, and bioconvection equations are given by Eqs. (5), (6), and (7), respectively. The Casson fluid model constitutes a number in the momentum boundary layer. Similarly, Maxwell fluid model instigates a number with three product-terms involving second-order derivatives. Hence, the first term and second term of the right-hand side of Eq. (3) explain the contribution of Casson and Maxwell fluids, respectively. The third term of the right-hand side of Eq. (3) is responsible for the involvement of magnetic field induction in the momentum boundary layer equation. The fourth, fifth, and sixth term of the right-hand side of Eq. (3) is thermal buoyancy force, species buoyancy effect, and motile density buoyancy effect, respectively [55]. In Eq. (4), the first two-term of the right-hand side are velocity gradients associated with horizontal and normal components of the induced magnetic field, whereas the third term is responsible for the diffusion of magnetic lines [53]. In Eq. (5), the second last term on the right-hand side is the offering of thermal radiation and the last term is the involvement of heat source/sinks. In Eq. (6), the last term is the contribution of chemical reactions. The third term of the left-hand side of Eq. (7) is showing the grant of Peclet number and motile density difference in the bioconvection effect.

Here u and v are the velocity components along x and y directions, respectively, T, C and s are fluid temperature, concentration and motile density, respectively, T_w is temperature at the wall, C_w is concentration at the wall, s_w is motile microorganisms density at the wall, H_1 and H_2 are horizontal and normal induced magnetic components, respectively, C_β is Casson parameter, λ_M is material parameter, μ_h is magnetic permeability, D_s is microorganisms diffusion, W_c is swimming cell speed, α_e is magnetic diffusivity, β_T, β_C, β_s are volumetric coefficients of thermal, solutal and motile density expansions, g^* is gravitation acceleration, R is reaction rate constant and b is chemotaxis constant. L_1, L_2, L_3 and L_4 are velocity, thermal, concentration and microorganism slip lengths, respectively. Eq. (3) gives the information about different cases of fluid flow. If λ_M=0, and $C_\beta\neq\infty$ then it is Casson fluid flow. Also for $C_\beta\to\infty$, and $\lambda_M\neq 0$, then it is Maxwell fluid flow. The Newtonian fluid can be obtained for $C_\beta\to\infty$, and λ_M=0. A complete sketch of the flow model is plotted in Fig. 1.

Following transformations are introduced:

$$\left.\begin{aligned} &u=axf',\ v=-\sqrt{a\upsilon}f(\eta),\ \eta=y\sqrt{\frac{a}{\upsilon}},\ \psi=x\sqrt{a\upsilon}f(\eta),\\ &\theta(\eta)=\frac{(T-T_\infty)}{(T_w-T_\infty)},\ \varphi(\eta)=\frac{(C-C_\infty)}{(C_w-C_\infty)},\ \chi(\eta)=\frac{(s-s_\infty)}{(s_w-s_\infty)},\\ &T=T_\infty(1+(\theta_w-1)\theta),\ \theta_w=\frac{T_w}{T_\infty},\\ &H_1=H_0xg'(\eta),\ H_2=-H_0\sqrt{\frac{\upsilon}{a}}g(\eta), \end{aligned}\right\} \tag{10}$$

where ψ is usual stream function with

$$u=\frac{\partial\psi}{\partial y}\ \text{and}\ v=-\frac{\partial\psi}{\partial x}. \tag{11}$$

Radiative heat flux is defined as:

$$q_r=-\frac{4\sigma^*}{3k^*}\frac{\partial T^4}{\partial y}. \tag{12}$$

.Eq. (12) is obtained from Rosseland approximation assuming the temperature difference between fluid particles being small. Beyond to the general case, here the emphasis is focused on the nonlinearity of thermal radiation. So, with the help of Eq.Eq. (12), the non-linear thermal radiation term $\frac{\partial q_r}{\partial y}$ in Eq. (5) is expressed as:

$$\frac{\partial q_r}{\partial y}=-\frac{16\sigma^*}{3k^*}\left[3T^2\left(\frac{\partial T}{\partial y}\right)^2+T^3\frac{\partial T^2}{\partial y^2}\right]. \tag{13}$$

Using transformations (10) with (11), the Eqs. (3)-(7) with Eq. (13) are finally reduced to:

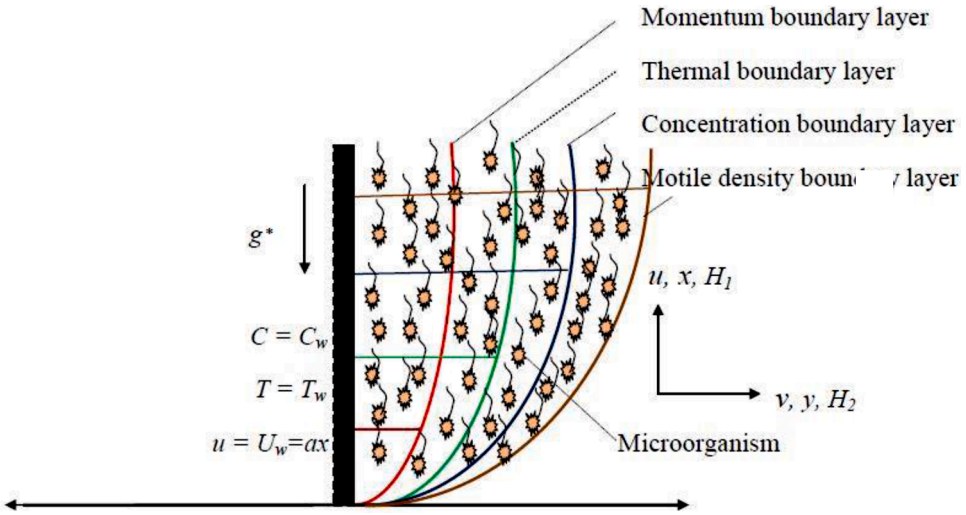

Fig. 1. The physical sketch of the problem.

$$\left(1+\frac{1}{C_\beta}\right)f''' - (')^2 + ff'' + M_\lambda\left(2ff'f'' - f^2f'''\right) + M^*\left((g')^2 - gg''\right) + \lambda\theta + \delta\varphi + \gamma\chi = 0, \tag{14}$$

$$g''' + \varepsilon(fg'' - f''g) = 0, \tag{15}$$

$$\theta'' + Nr\theta''\left[1+\left(\theta_w^*-1\right)\theta\right]^3 + 3Nr\theta'^2\left(\theta_w^*-1\right)\left[1+\left(\theta_w^*-1\right)\theta\right]^2 + \Pr(f\theta' + Q_0\theta) = 0, \tag{16}$$

$$\varphi'' + Scf\varphi' - RcSc\varphi = 0, \tag{17}$$

$$\chi'' + Lbf\chi' - Pe[\varphi''(\chi+\Omega) + \varphi'\chi'] = 0, \tag{18}$$

where

$\lambda = \frac{Gr_T}{\mathrm{Re}_x^2}, \delta = \frac{Gr_C}{\mathrm{Re}_x^2}$, $\gamma = \frac{Gr_s}{\mathrm{Re}_x^2}, Gr_T = \frac{g\beta_T(T_w-T_\infty)x^3}{\upsilon^2}, Gr_C = \frac{g\beta_C(C_w-C_\infty)x^3}{\upsilon^2}$, $Gr_s = \frac{g\beta_s(s_w-s_\infty)x^3}{\upsilon^2}$, $M_\lambda = \lambda_M a$, $Nr = \frac{16\sigma^*T_\infty^3}{3kk^*}, \theta_w^* = \frac{T_w}{T_\infty}, Sc = \frac{\upsilon}{D_B}, Lb = \frac{\upsilon}{D_s}, Pe = \frac{bW_c}{D_s}, Rc = \frac{R}{a}, \Pr = \frac{\upsilon}{\alpha_1}, \varepsilon = \frac{\upsilon}{\alpha_e}, M^* = \frac{\mu_h}{4\pi\rho}\left(\frac{H_0}{a}\right)^2, \Omega = \frac{s_w}{s_w-s_\infty}$ and $Q_0 = \frac{Q}{a\rho c_p}$ are thermal, solutal and microorganism buoyancy parameters, thermal, solutal and microorganism Grashof numbers, Deborah number (Maxwell fluid parameter), thermal radiation parameter, temperature ratio parameter, Schmidt number, bioconvection Lewis number, Peclet number, reaction rate parameter, Prandtl number, magnetic Prandtl number, induced magnetic number, microorganism concentration difference parameter and heat generation/absorption parameter, respectively.

From Eqs. (8) and (9), the corresponding boundary conditions are

$$\left.\begin{array}{l} f(0)=0,\ f'(0)=1+\lambda_1 f''(0),\ \theta(0)=1+\lambda_2\theta'(0), \\ \varphi(0)=1+\lambda_3\varphi'(0),\ \chi(0)=1+\lambda_4\chi'(0),\ g(0)=0=g''(0), \\ f'(\infty)=0,\ \theta(\infty)=0,\ \varphi(\infty)=0,\ \chi(\infty)=0,\ g'(\infty)=1, \end{array}\right\} \tag{19}$$

where $\lambda_1 = L_1\sqrt{\frac{a}{\upsilon}}$, $\lambda_2 = L_2\sqrt{\frac{a}{\upsilon}}$, $\lambda_3 = L_3\sqrt{\frac{a}{\upsilon}}$ and $\lambda_4 = L_4\sqrt{\frac{a}{\upsilon}}$ is velocity, thermal, solutal and motile microorganism density slip parameters.

For engineering purposes, the physical quantities of interest, local skin-friction coefficient, local Nusselt number, local Sherwood and motile density numbers are defined in their usual forms as:

$$C_f = \frac{(\tau_w)_{y=0}}{\rho U_w^2}, \quad Nu = \frac{x(q_w)_{y=0}}{k(T_w-T_\infty)}, \quad Sh = \frac{x(j_w)_{y=0}}{D_M(C_w-C_\infty)}, \quad Bh = \frac{x(p_w)_{y=0}}{D_s(s_w-s_\infty)}. \tag{20}$$

Here, τ_w, q_w, j_w, p_w are wall shear stress, heat flux, mass flux and motile flux, respectively and expression of such quantities are given as:

$$(\tau_w)_{y=0} = (1+M_\lambda)\left(1+\frac{1}{C_\beta}\right)\mu\left(\frac{\partial u}{\partial y}\right)_{y=0}, \quad (q_w)_{y=0} = -k\left(\frac{\partial T}{\partial y}\right)_{y=0} + (q_r)_{y=0}, \quad (j_w)_{y=0} = -D_B\left(\frac{\partial C}{\partial y}\right)_{y=0}, \quad (p_w)_{y=0} = -D_s\left(\frac{\partial s}{\partial y}\right)_{y=0}.$$

Dimensionless expressions for skin-friction factor, reduced Nusselt number, reduced Sherwood number and reduced motile density number are

$\mathrm{Re}_x^{1/2}C_f = f''(0)(1+M_\lambda)\left(1+\frac{1}{C_\beta}\right)$, $\mathrm{Re}_x^{-1/2}Nu = -(1+Nr\theta_w^{*3})\theta'(0)$, $\mathrm{Re}_x^{-1/2}Sh = -\varphi'(0)$, and $\mathrm{Re}_x^{-1/2}Bh = -\chi'(0)$, where $\mathrm{Re}_x = \frac{xU_w}{\upsilon}$ is local Reynolds number.

3. Solution methodology

Eqs. (14)-(18) associated with conditions (19) are solved by 'bvp4c' [56–59], a MATLAB package. The primary step in this method is to transform the boundary value problem (BVP) into an initial value problem (IVP) having first order system of ODEs. The asymptotically convergent solutions with obeying specified tolerance level of 10^{-6} are achieved taking a finite value of infinite boundary, $\eta\to\infty$, say $\eta_\infty(=12)$, by integrating following first-order system given by:

$$y_3' = \frac{y_2^2 - y_1y_3 - 2M_\lambda y_1y_2y_3 - M^*\left(y_{11}^2 - y_{10}y_{12}\right) - \lambda y_4 - \delta y_6 - \gamma y_8}{\left(1+\frac{1}{C_\beta} - M_\lambda y_1^2\right)},$$

$$y_5' = \frac{-3Nr(y_5)^2\left(\theta_w^*-1\right)\left[1+\left(\theta_w^*-1\right)y_4\right]^2 - \Pr(y_1y_5 + Q_0y_4)}{\left(1+Nr\left[1+\left(\theta_w^*-1\right)y_4\right]^3\right)},$$

$$y_7' = -Scy_1y_7 + RcScy_6,$$

$$y_9' = -Lby_1y_9 + Pe[(-Scy_1y_7 + RcScy_6)(y_8+\Omega) + y_7y_9],$$

$$y_{12}' = -\varepsilon(y_1y_{12} - y_{10}y_3),$$

where $f = y_1, f' = y_2, f'' = y_3, \theta = y_4, \theta' = y_5, \varphi = y_6, \varphi' = y_7, \chi = y_8, \chi' = y_9, g = y_{10}, g' = y_{11}, g'' = y_{12}$ with relative boundary conditions

$y_1(0)=0$, $y_2(0)=1+\lambda_1y_3(0)$, $y_4(0)=1+\lambda_2y_5(0)$, $y_6(0)=1+\lambda_3y_7(0)$, $y_8(0)=1+\lambda_4y_9(0)$, $y_{10}(0)=0$, $y_{12}(0)=0$, $y_2(\infty)=0$, $y_4(\infty)=0$, $y_6(\infty)=0$, $y_8(\infty)=0$, $y_{11}(\infty)=1$.

4. Results and discussion

We explore a comparative discussion of two different types of non-Newtonian fluids (i.e., Maxwell and Casson fluids) with the assumption of the same physical aspects. To confirm the correctness of the MATLAB inbuilt function, 'bvp4c', we compare our calculated value $-\theta'(0)$ for several values of Pr with the results of Hassanien et al. [60], Salleh and Nazar [61] and Ali et al. [62] and it is noted that those have a good agreement; all things are given in Table 1.

The whole analysis is discussed with Maxwell fluid (M_λ=0.3) and Casson fluid (C_β = 5.0). The fixed values of parameters considered to show impact of certain parameters on $f'(\eta)$, $g'(\eta)$, $\theta(\eta)$, $\varphi(\eta)$ and $\chi(\eta)$ are considered as λ=0.01, δ=0.01, γ=0.01, M^*=0.001, Pr = 3.0, Q_0=0.1, Nr=0.2, θ_w^* = 1.2, Sc=1.0, Rc=0.6, Pe=0.5, Ω=0.4. The velocity, magnetic induction, temperature, concentration, and motile density profiles are explored with distinct values of the involved parameters. Fig. 2(a)-(c) illustrates the impact of M^* on magnetic induction, velocity, and motile density profiles. Observation from these reveals that with higher M^*, magnetic induction enhances near sheet and away from it, the contrary impact is witnessed. It can be also observed in this image that with induced magnetic number the flow velocity escalates, whereas motile density falls with M^*. Actually, the directions of applied and induced magnetic fields are opposite and so consideration of induced magnetic field improves flow drag and velocity enhances. One can observe that the velocity of Maxwell fluid is quantitatively lesser than the velocity of Casson fluid. The motile density decreases, which can be observed from this figure and moreover the motile density of Maxwell

Table 1
Comparison of the values of $-\theta'(0)$ for various Pr.

Pr	Hassanien et al. [60]	Salleh and Nazar [61]	Ali et al. [62]	Current investigation
0.72	0.46325	0.46317	0.4632	0.4632515
1.0	0.58198	0.58198	0.5820	0.5819813
3.0	1.16525	1.16522	1.1652	1.1652455
10.0	2.30801	2.30821	2.3081	2.3080057

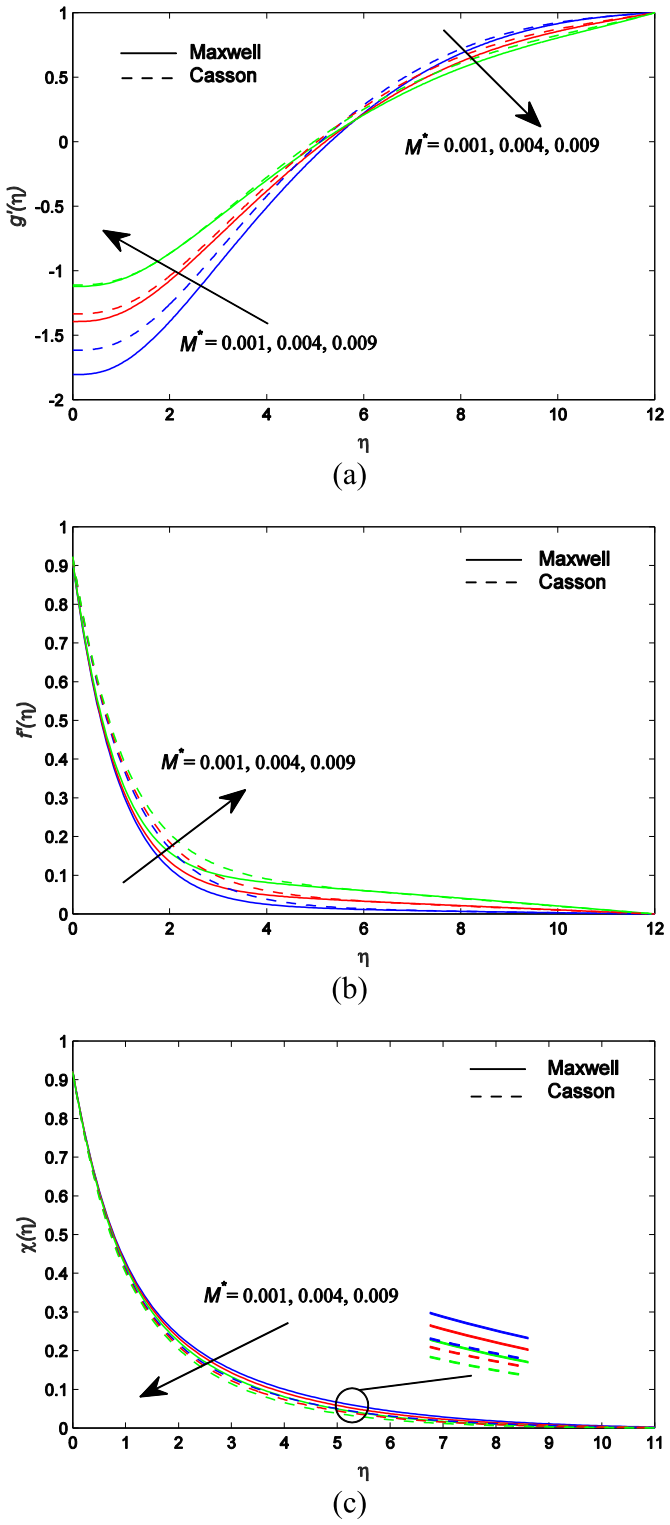

Fig. 2. Impacts of M on (a) magnetic induction, (b) velocity, and (c) motile density.

fluid is higher than Casson fluid. Fig. 3(a)-(c) exhibits the impacts of thermal buoyancy parameter on $g'(\eta)$, $f'(\eta)$ and $\theta(\eta)$. It suggests that $g'(\eta)$ decreases for assisting flow ($\lambda>0$) for smaller value of η and increases in higher value of η, whereas $g'(\eta)$ increases in opposing flow ($\lambda<0$) for smaller value of η and decreases in the case of larger value of η. It also demonstrates that when λ increases, velocity grows, i.e., for aiding flow ($\lambda>0$) it rises and for opposing flow ($\lambda<0$) it decreases. The reason for this is that for positive λ, a favorable pressure gradient is generated, which accelerates the motion, and for negative λ, the opposite scenario occurs. The buoyancy impact is significantly stronger for opposing flows ($\lambda<0$) than for aiding flows($\lambda>0$). Additionally, it is also observe that Casson fluid have higher magnetic induction and higher velocity than Maxwell fluid from quantitative point of view in both situation, i.e. for near the surface and for away from the surface, whereas temperature profile shows reveres trend, i.e., for Maxwell fluid higher temperature distribution is obtained than Casson fluid. Fig. 4(a)-(b) portrays the

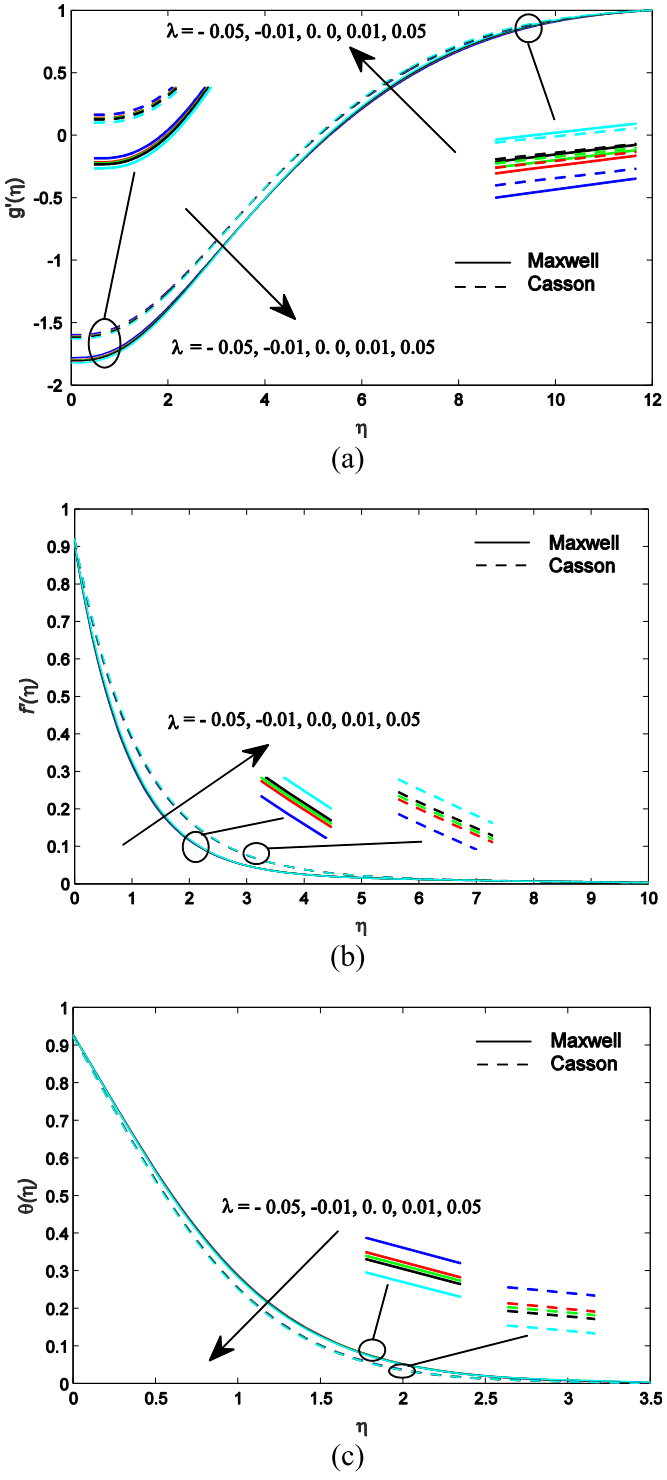

Fig. 3. Impacts of λ on (a) magnetic induction, (b) velocity, and (c) temperature.

influence of γ to motile density and velocity profiles. Physically, the larger value of γ is attributable to the buoyant force owing to bio-convection, which results in an increase in velocity, whereas motile density shows decreasing trend for enhancing the value of γ. From quantitative point of view, it can be summarized that motile density is higher for Maxwell fluid and lesser for Casson fluid. Fig. 5(a)-(c) depicts that velocity increases when ε increases. It can be seen that as magnetic Prandtl number, ε increases, induced magnetic field at the surface is also increased, whereas motile density is showing different behaviour. Figure Fig. 6(a)-(c) explains the significant impact of Nr, θ_w^* and heat generation/absorption on temperature profile. It is noteworthy that temperature displays increasing trends as the values of Nr and θ_w^* increase. This is because, as the radiation parameter is at increased level, more heat is transferred to the fluid, causing a considerable increment in temperature inside the boundary layer. It depicts from the figure that temperature displays increasing trends as the values of Nr rises. From this, it is also obtained that when heat generation ($Q_0>0$) occurs, nature of thermal state of fluid goes to higher level and it helps to the growth of temperature boundary layer. Enhancement in heat absorption($Q_0<0$), temperature profile is influenced oppositely. Fig. 7(a)-(c) shows that as the higher values of concentration slip parameter causes the reduction of concentration distribution inside the boundary layer, whereas density of microbes is showing contrary nature. It is also observed that enhancement in the value of velocity slip parameter magnetic induction rises close to sheet and declines for away from it. From graph, it witnesses

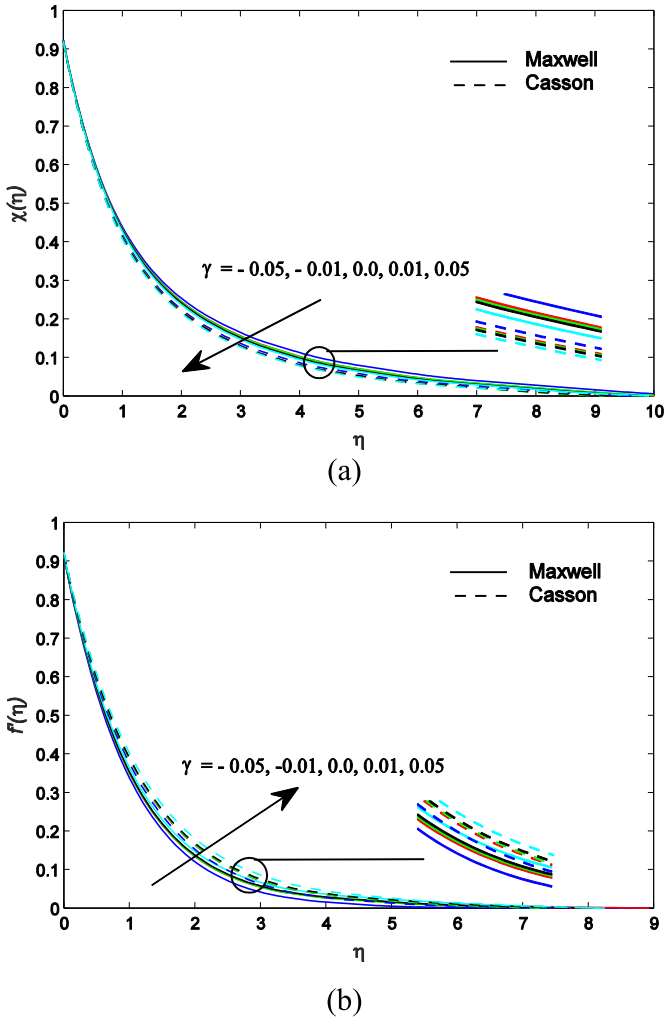

Fig. 4. Effects of motile buoyancy parameter on (a) motile density, and (b) velocity.

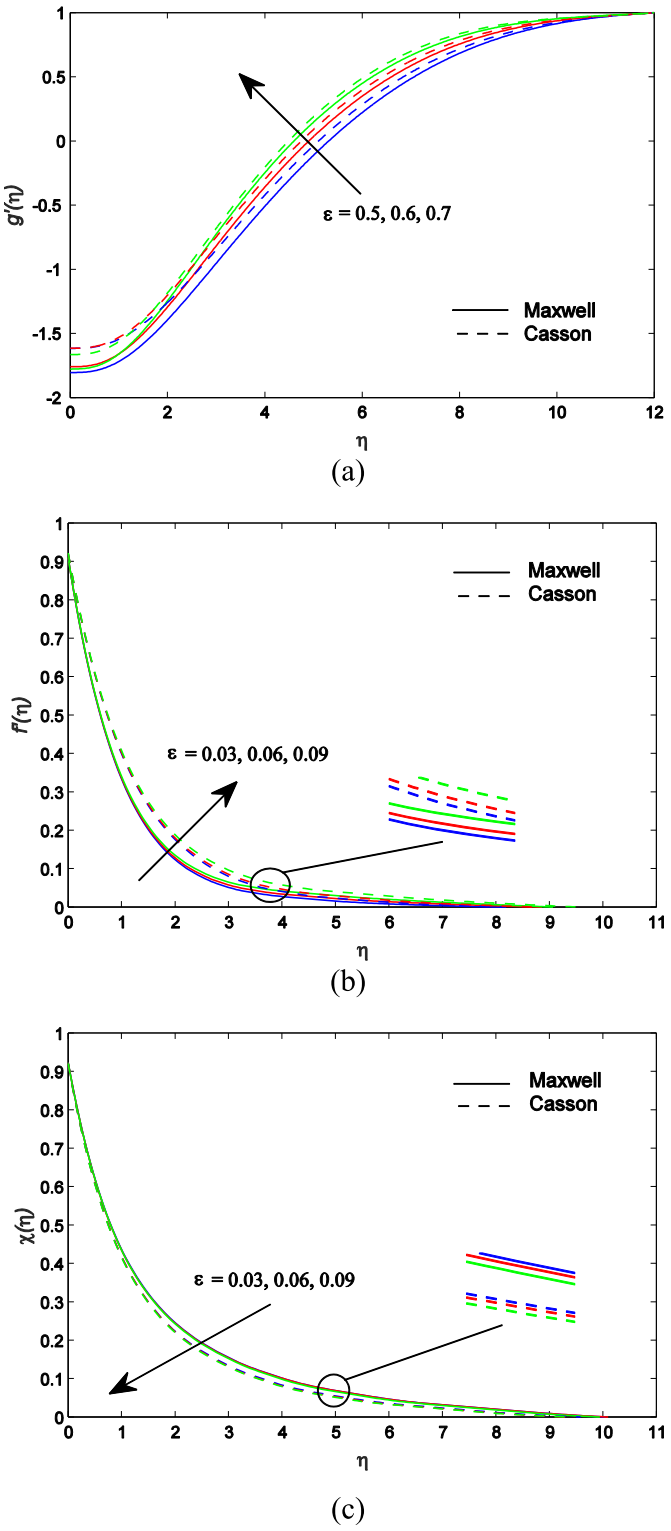

Fig. 5. Effects of magnetic Prandtl number on (a) magnetic induction, (b) velocity, and (c) motile density.

that as velocity slip parameter increases, the temperature, concentration and motile density also increase. Fig. 8(a)-(c) depicts the nature of magnetic induction and motile density profiles for several Pe and Ω. Increment in the microorganism density difference, the magnetic induction profile for Casson fluid is more prominent than Maxwell fluid. The intrinsic energy of microorganisms is used to establish the bio-convection principle and the density of motile microorganisms is

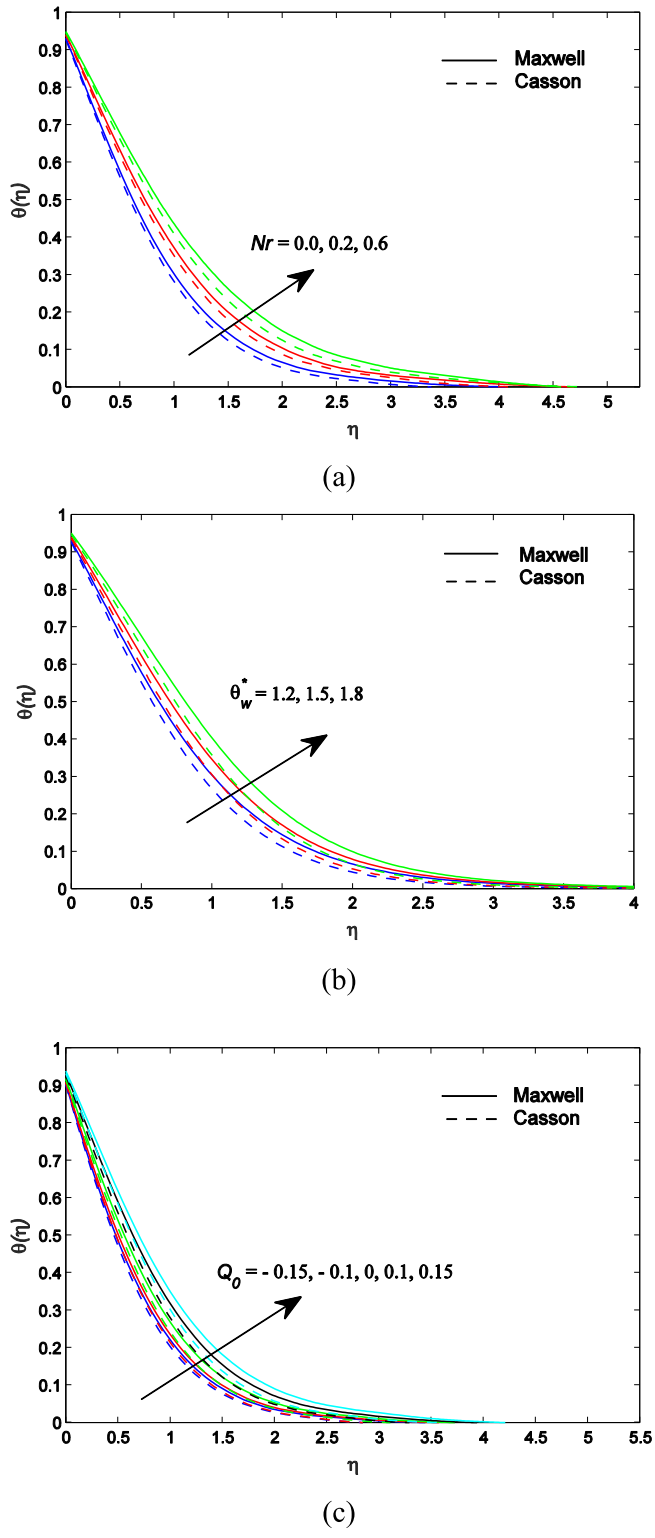

Fig. 6. Effects of (a) *Nr*, (b) Q_0, and (c) θ_W on temperature.

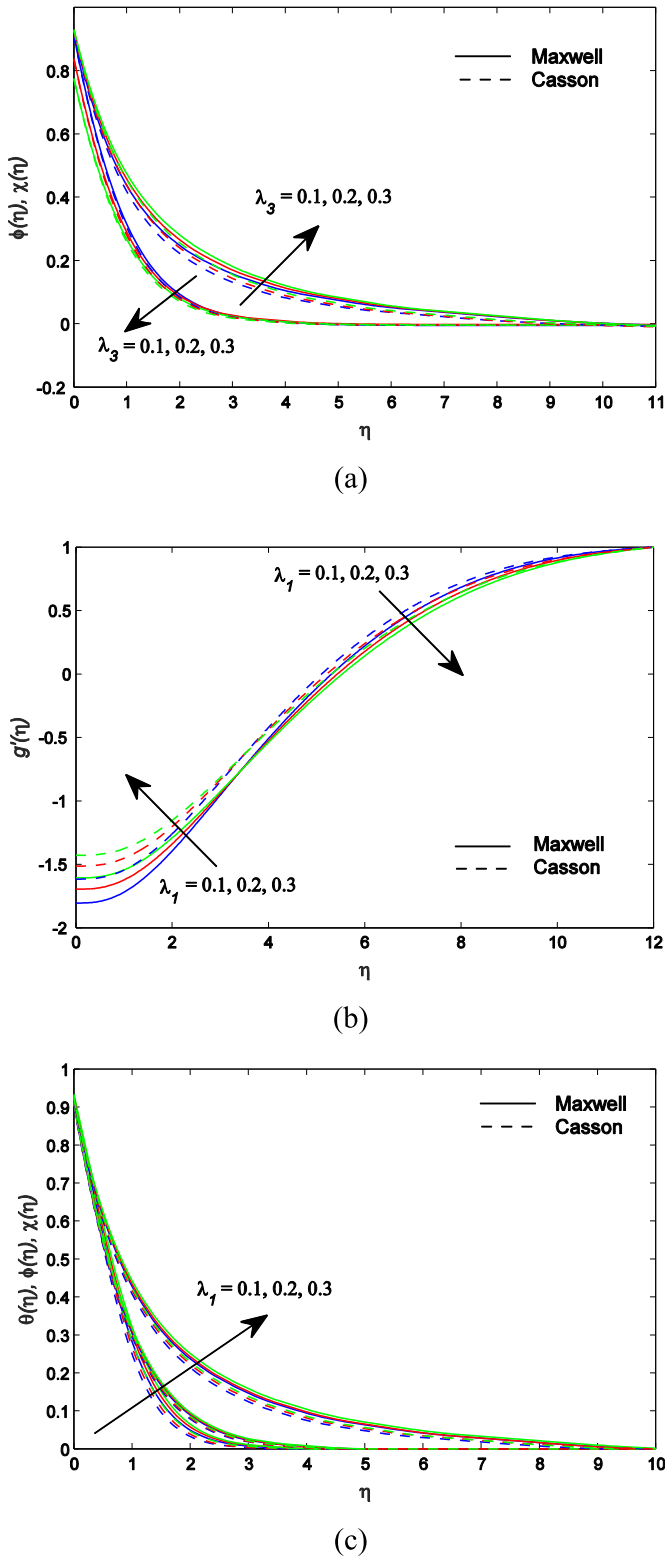

Fig. 7. Effects of (a) concentration slip on concentration and motile density, (b) velocity slip on magnetic induction, and (c) velocity slip on temperature, concentration and motile density.

severely influenced by the values of *Pe* and Ω. Also, motile bacteria have a high propulsion rate due to their self-motivated motility. Since *Pe* is inversely proportional to motile density, as a result, a higher fluctuation in *Pe* translates to a lower motile density, which causes drop in motile density profile, i.e., when *Pe* increases, the density of microorganisms falls. From this figure, one can observe the fact that for higher *Pe* values, the motile bacteria swims slower. From this figure, it is notable that with increasing motile density difference ratio Ω there is a decrement in the motile density of microorganism, which is similar like *Pe*. From this figure one significant feature of motile density profile is visible for comparison of Maxwell and Casson fluid. For larger value of Ω and *Pe* and smaller η motile density is higher for Maxwell fluid than Casson fluid, but for larger involvement of η the motile density of Casson fluid

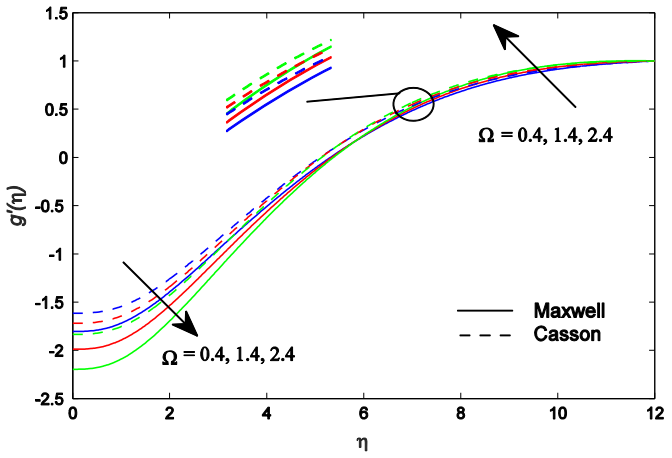

(a)

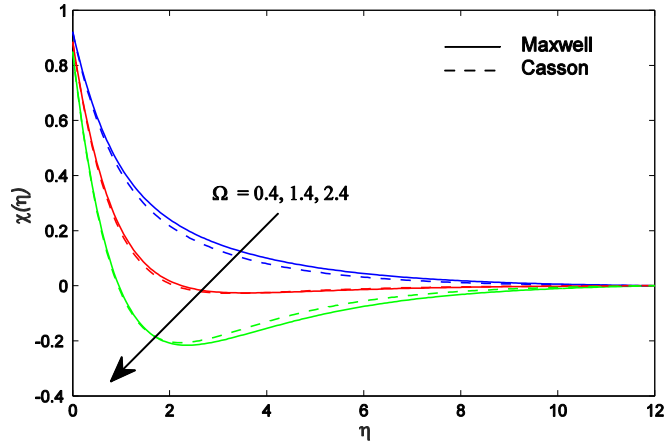

(b)

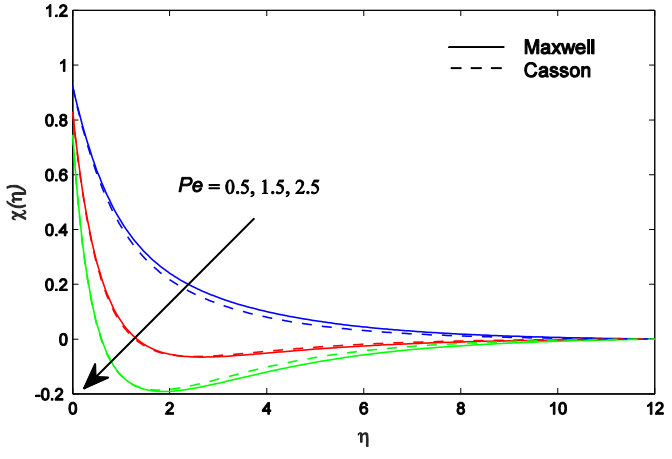

(c)

Fig. 8. Effects of (a) microorganism difference ratio on magnetic induction (b) microorganism difference ratio on motile density, and (c) Peclet number on motile density.

significantly grow up in comparison of Maxwell fluid. Fig. 9(a)-(c) shows variation in Nusselt number with Q_0 and *Nr*, variations in skin-friction, and motile density number with *Pe* and Ω. It has been observed that increasing *Nr* causes growth in heat transfer rate (Nusselt number), whereas increasing value of Q_0 causes reduction in heat transfer rate. It is also witnessed that motile density number shows growth with *Pe* and Ω, but wall drag-force exhibits opposite character. The same influences in local Nusselt number, skin-friction coefficient and motile density number for Maxwell fluid and Casson fluid are separately calculated and shown in tabular form by Tables 2-4.

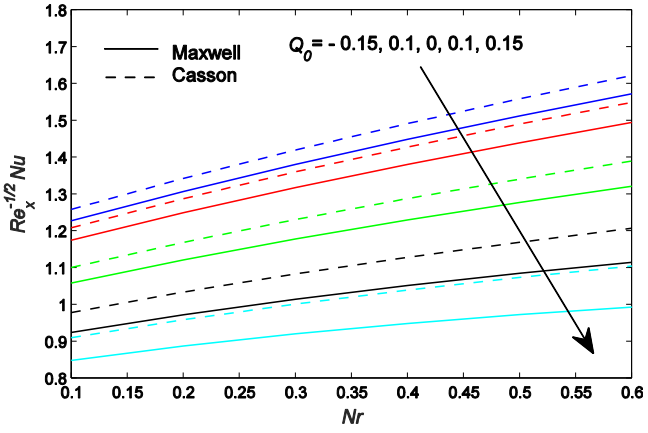

(a)

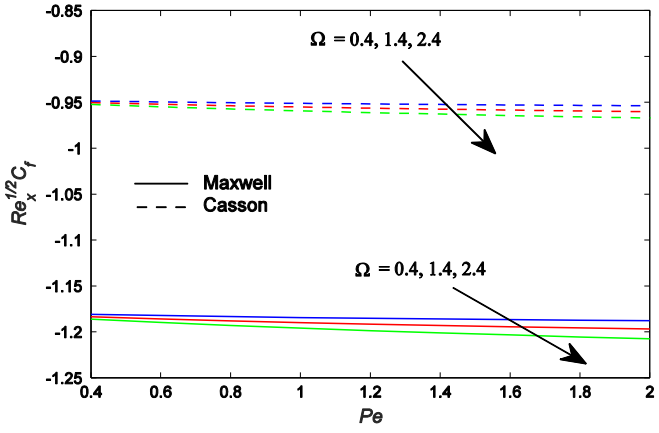

(b)

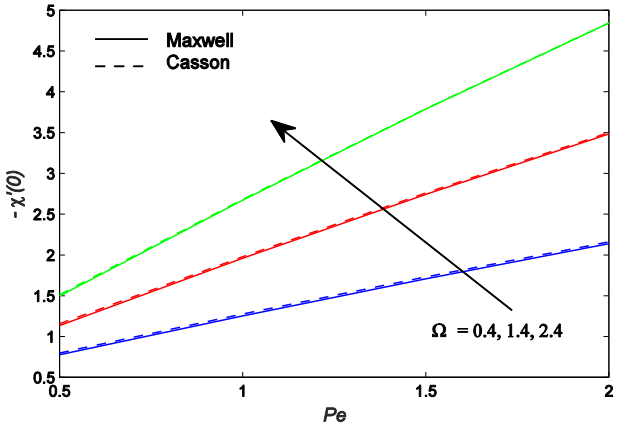

(c)

Fig. 9. Variations in (a) Nusselt number with Q_0 and *Nr* (b) skin-friction with *Pe* and Ω, and (c) motile density number with *Pe* and Ω.

5. Conclusions

From the above comparative investigation on bioconvective induced MHD flow of Maxwell and Casson fluids in presence of multiple slips, heat source/sink and nonlinear thermal radiation, several novel and significant remarks about velocity, temperature, concentration and motile density organism profiles are obtained and those can be summarized as:

- With induced magnetic number, velocity rises and motile density microorganism drops. While comparing Maxwell fluid to Casson fluid, the Casson fluid velocity is more noticeable than the Maxwell fluid velocity.
- For enhancement in assisting thermal buoyancy, velocity grows up and motile density velocity slides down, whereas for similar enhancement in opposing thermal buoyancy, contrary natures of velocity and microbe density are noticed.
- For hiked value of magnetic Prandtl number, magnetic induction and velocity shows increasing trend, but microorganism density profile is showing different nature.
- Increasing the amounts of *Pe* and Ω significantly reduces the motile density profile. When Maxwell fluid and Casson fluid are compared, then it is found that motile density profile for Maxwell fluid is more projecting than the profile for Casson fluid.
- The temperature, concentration and motile density increase with velocity slip, whereas magnetic induction rises near plate and declines away from it. In case of increasing concentration slip parameter, the natures of concentration and motile density are conflicting.
- As the value of thermal radiation rises, the temperature rises with it. Also, for higher temperature difference ratio and heat generation parameter temperature exhibits growing behaviour; however for heat absorption it shows the opposite tendency.
- The behaviour of microorganism motile profile for large Ω and with smaller η is more prominent for Maxwell fluid than Casson fluid. But, for larger η microorganism motile for Casson fluid is greater than Maxwell fluid. Similar nature of microorganism motile profile is obtained for the big value of *Pe*.
- The heat transfer rate is significantly rises with enhancing the value of thermal radiation parameter.
- Motile density number and skin friction coefficient decrease with increasing Peclet number and motile density difference parameter for both fluids, i.e., for Maxwell and Casson fluids. Additionally, Casson fluid have higher motile density number than Maxwell fluid.

Table 2
Variations in skin-friction with Peclet number and microorganism density parameter.

Parameters		$\mathrm{Re}_x^{1/2}C_f$	
Ω	Pe	Maxwell fluid	Casson fluid
0.4	0.4	-1.1809773	-0.9486683
	0.6	-1.1822228	-0.9495880
	0.8	-1.1833285	-0.9504061
	1.0	-1.1843102	-0.9511343
	1.2	-1.1851821	-0.9517830
	1.4	-1.1859573	-0.9523616
	1.6	-1.1866473	-0.9528784
	1.8	-1.1872625	-0.9533409
	2.0	-1.1878120	-0.9537555
1.4	0.4	-1.1835008	-0.9505178
	0.6	-1.1858556	-0.9522380
	0.8	-1.1879762	-0.9537825
	1.0	-1.1898843	-0.9551688
	1.2	-1.1916007	-0.9564137
	1.4	-1.1931449	-0.9575323
	1.6	-1.1945346	-0.9585388
	1.8	-1.1957869	-0.9594456
	2.0	-1.1969167	-0.9602641
2.4	0.4	-1.1860920	-0.9523944
	0.6	-1.1896379	-0.9549449
	0.8	-1.1928829	-0.9572520
	1.0	-1.1958530	-0.9593376
	1.2	-1.1985722	-0.9612228
	1.4	-1.2010639	-0.9629272
	1.6	-1.2033501	-0.9644692
	1.8	-1.2054516	-0.9658659
	2.0	-1.2073877	-0.9671328

Table 3
Variations in Nusselt number with heat generation/absorption and thermal radiation parameters.

Parameters		$\mathrm{Re}_x^{-1/2}Nu$	
Q_0	*Nr*	Maxwell	Casson
−0.15	0.1	1.2266090	1.2577767
	0.2	1.3067345	1.3418765
	0.3	1.3801843	1.4191916
	0.4	1.4482045	1.4909763
	0.5	1.5116997	1.5581409
	0.6	1.5713514	1.6213711
−0.1	0.1	1.1737866	1.2078842
	0.2	1.2485159	1.2870167
	0.3	1.3167984	1.3595962
	0.4	1.3798349	1.4268310
	0.5	1.4384980	1.4895983
	0.6	1.4934456	1.5485591
0.0	0.1	1.0578721	1.0996653
	0.2	1.1204827	1.1678856
	0.3	1.1770684	1.2300032
	0.4	1.2287364	1.2871306
	0.5	1.2762931	1.3400762
	0.6	1.3203487	1.3894501
0.1	0.1	0.9238392	0.9772657
	0.2	0.9716962	1.0327907
	0.3	1.0138028	1.0826043
	0.4	1.0511608	1.1277153
	0.5	1.0845021	1.1688571
	0.6	1.1143815	1.2065839
0.15	0.1	0.8474802	0.9091994
	0.2	0.8863896	0.9574234
	0.3	0.9195362	1.0000778
	0.4	0.9478533	1.0381140
	0.5	0.9720188	1.0722210
	0.6	0.9925437	1.1029178

Table 4
: Variations in motile density number with Peclet number and microorganism density parameter.

Parameter		$-\chi'(0)$	
Ω	Pe	Maxwell	Casson
0.4	0.5	0.7743855	0.7980825
	1.0	1.2529710	1.2754311
	1.5	1.7070644	1.7295884
	2.0	2.1360772	2.1595209
1.4	0.5	1.1347959	1.1552612
	1.0	1.9598496	1.9769027
	1.5	2.7434668	2.7594623
	2.0	3.4840274	3.5007071
2.4	0.5	1.4962840	1.5130806
	1.0	2.6704438	2.6803701
	1.5	3.7869710	3.7927972
	2.0	4.8426847	4.8466387

Funding Information

The authors have no grant to be acknowledged.

Declaration of interests

The authors declare that they have no known competing financial interests or personal relationships that could have appeared to influence the work reported in this paper.

Acknowledgement

The authors are thankful to the esteemed reviewers for their constructive and valuable suggestions.

References

[1] J.C. Maxwell, On the dynamical theory of gases, Proc. R. Soc. London 15 (1866) 167–171.
[2] T. Hayat, M. Qasim, Influence of thermal radiation and Joule heating on MHD flow of a Maxwell fluid in the presence of thermophoresis, Int. J. Heat Mass Transf. 53 (2010) 4780–4788.
[3] T. Hayat, R. Sajjad, Z. Abbas, M. Sajid, A. Hendi, Radiation effects on MHD flow of Maxwell fluid in a channel with porous medium, Int. J. Heat Mass Transf. 54 (2011) 854–862.
[4] S. Shateyi, A new numerical approach to MHD flow of a Maxwell fluid past a vertical stretching sheet in the presence of thermophoresis and chemical reaction, Bound. Value Probl. 2013 (2013), 196.
[5] S. Mukhopadhyay, Heat transfer analysis of the unsteady flow of a Maxwell fluid over a stretching surface in the presence of a heat source/sink, Chinese Phys. Lett. 29 (5) (2012), 054703.
[6] N. Casson, A flow equation for pigment-oil suspensions of the printing ink type, in: C.C. Mill (Ed.), Rheology of Disperse Systems, Pergamon Press, Oxford, 1959, pp. 84–104.
[7] A.G. Fredrickson, Principles and Applications of Rheology, Prentice-Hall. Englewood Cliffs, 1964, pp. 16–23.
[8] A.V. Mernone, J.N. Mazumdar, S.K. Lucas, A mathematical study of peristaltic transport of a Casson fluid, Math. Comput. Model. 35 (7-8) (2002) 895–912.
[9] P.S. Gupta, A.S. Gupta, Heat and mass transfer on a stretching sheet with suction or blowing, Can. J. Chem. Eng. 55 (6) (1977) 744–746.
[10] I. Pop, T. Na, Unsteady flow past a stretching sheet, Mech. Res. Commun. 23 (4) (1996) 413–422.
[11] A. Ishak, Similarity solutions for flow and heat transfer over a permeable surface with convective boundary condition, Appl. Math. Comput. 217 (2010) 837–842.
[12] M.A.A. Hamad, Analytical solution of natural convection flow of a nanofluid over a linearly stretching sheet in the presence of magnetic field, Int. Commun. Heat Mass Transf. 38 (4) (2011) 487–492.
[13] S. Pramanik, Casson fluid flow and heat transfer past an exponentially porous stretching surface in the presence of thermal radiation, Ain Shams Eng. J. 5 (1) (2014) 205–212.
[14] P.K. Rameswaran, S. Shaw, P. Sibanda, Dual solutions of Casson fluid flow over stretching or shrinking sheet, Sādhāna 39 (6) (2014) 1573–1583.
[15] K. Bhattacharyya, T. Hayat, A. Alsaedi, Exact solution for boundary layer flow of Casson fluid over a permeable stretching/shrinking sheet, J. Appl. Math. Mech. 94 (6) (2014) 522–528.
[16] K. Bhattacharyya, T. Hayat, A. Alsaedi, Analytical solution for magnetohydrodynamic boundary layer flow of Casson fluid over a stretching/shrinking sheet with wall mass transfer, Chin. Phys. B 22 (2) (2013), 224702.
[17] S. Mukhopadhyay, P.R. De, K. Bhattacharyya, G.C. Layek, Casson fluid flow over an unsteady stretching surface, Ain Shams Eng. J. 4 (4) (2013) 933–938.
[18] J. Boyd, J.M. Buick, S. Green, Analysis of the Casson and Carreau-Yasuda non-Newtonian blood models in steady and oscillatory flows using the lattice Boltzmann method, Phys. Fluids 19 (2007), 093103.
[19] M.S. Kumar, N. Sandeep, B.R. Kumar, S. Saleem, A comparative study of chemically reacting 2D flow of Casson and Maxwell fluids, Alexandria Eng. J. 57 (3) (2018) 2027–2034.
[20] G. Kumaran, N. Sandeep, M.E. Ali, Computational analysis of magnetohydrodynamics Casson and Maxwell flows over a stretching sheet with cross diffusion, Results Phys. 7 (2017) 147–155.
[21] Z. Shah, A. Dawar, S. Islam, A. Alshehri, H. Alrabaiah, A comparative analysis of MHD Casson and Maxwell flows past a stretching sheet with mixed convection and chemical reaction, Waves Random Complex Media (2021) 1-16 10.1080/17455030.2021.2004333.
[22] C.L.M.H. Navier, Mémoire sur les lois du mouvement des fluides. Mem, The French Academy Institut des, Sciences 2 (1823) 389–440.
[23] J.C. Maxwell, On stresses in rarefied gases arising from inequalities of temperature, Phil. Trans. R. Soc. 170 (1879) 231–256.
[24] H.I. Andersson, Slip flow past a stretching surface, Acta Mech. 158 (2002) 121–125.
[25] K. Bhattacharyya, G.C. Layek, Slip effect on diffusion of chemically reactive species in boundary layer flow over a vertical stretching sheet with suction or blowing, Chem. Eng. Commun. 198 (11) (2011) 1354–1365.
[26] M.M. Bhatti, O.A. Beg, I.A. Abdelsalam, Computational framework of magnetized MgO–Ni/water-based stagnation nanoflow past an elastic stretching surface: Application in solar energy coatings, Nanomaterials 12 (7) (2022) 1049.
[27] M.I. Khan, F. Alzahrani, Entropy-optimized dissipative flow of Carreau-Yasuda fluid with radiative heat flux and chemical reaction, Eur. Phys. J. Plus 135 (6) (2020) 516.
[28] S. Mukhopadhyay, R.S.R. Gorla, Effects of partial slip on boundary layer flow past a permeable exponential stretching sheet in presence of thermal radiation, Heat Mass Transf. 48 (2012) 1773–1781.
[29] Y. Chu, S. Aziz, M.I. Khan, M. Nazeer, I. Ahmad, I. Tlili, Nonlinear radiative bioconvection flow of Maxwell nanofluid configured by bidirectional oscillatory moving surface with heat generation phenomenon, Phys. Scr. 95 (2020), 105007.
[30] M. Ramzan, J.D. Chung, N. Ullah, Radiative magnetohydrodynamics nanofluid flow due to gyrotactic microorganisms with chemical reaction and non-linear thermal radiation, Int. J. Mech Sci. 130 (2017) 31–40.
[31] A.S. Alshomrani, M.Z. Ullah, D. Baleanu, Importance of multiple slips on bioconvection flow of cross nanofluid past a wedge with gyrotactic motile microorganisms, Case Stud. Therm. Eng. 22 (2020), 100798.
[32] M.I. Khan, M. Waqas, T. Hayat, M.I. Khan, A. Alsaedi, Behavior of stratification phenomenon in flow of Maxwell nanomaterial with motile gyrotactic microorganisms in the presence of magnetic field, Int. J. Mech. Sci. 131-132 (2017) 426–434.
[33] R. Katta, S.U. Khan, M. Jameel, M.I. Khan, Y.M. Chu, S. Kadry, Bioconvection assessment in Maxwell nanofluid configured by a Riga surface with nonlinear thermal radiation and activation energy, Surf. Interfaces 21 (2020), 100749.
[34] Y.M. Chu, B.M. Shankaralingappa, B.J. Gireesha, Faris Alzahrani, M.I. Khan, S. U. Khan, Combined impact of Cattaneo-Christov double diffusion and radiative heat flux on bioconvective flow of Maxwell liquid configured by a stretched nanomaterial surface, Appl. Math. Comput. 419 (2022), 126883.
[35] A. Shahid, M.M. Bhatti, R. Ellahi, K.S. Mekheimer, Numerical experiment to examine activation energy and bio-convection Carreau nanofluid flow on an upper paraboloid porous surface: application in solar energy, Sustain. Energ. Tech. Assessm. 52 (A) (2022), 102029.
[36] K. Al-Khaled, S.U. Khan, Thermal aspects of Casson nanoliquid with gyrotactic microorganisms, temperature dependent viscosity and variable thermal conductivity: Bio-technology and thermal applications, Inventions 5 (3) (2020) 39.
[37] S.U. Khan, H. Ali, Swimming of gyrotactic microorganisms in unsteady flow of Eyring Powell nanofluid with variable thermal features: bio-technology applications, Int. J. Thermophys. 41 (2020) 159.
[38] S.U. Khan, K. Al-Khaled, M.I. Khan, Convective nonlinear thermally developed flow of thixotropic nanoliquid configured by Riga surface with gyrotactic microorganism and activation energy: A bio-technology and thermal extrusion model, Int. Commun. Heat Mass Transf. 119 (2020), 104966.
[39] S.U. Khan, I. Tlili, Significance of activation energy and effective Prandtl number in accelerated flow of Jeffrey nanoparticles with gyrotactic microorganisms, J. Energ. Resources Tech. 142 (2020), 112101.
[40] M.M. Bhatti, M.B. Arain, A. Zeeshan, R. Ellahi, M.H. Doranehgard, Swimming of Gyrotactic Microorganism in MHD Williamson nanofluid flow between rotating circular plates embedded in porous medium: Application of thermal energy storage, J. Energ. Storage 45 (2022), 103511.
[41] O.K. Koriko, N.A. Shah, S. Saleem, J.D. Chung, A.J. Omowaye, T. Oreyeni, Exploaration of bioconvection flow of MHD thixotropic nanofluid past a vertical surface coexisting with both nanoparticles and gygrotactic microorganism, Sci. Rep. 17 11 (1) (2021) 16627.
[42] Q. Shi, A. Hamid, M.I. Khan, R.N. Kumar, R.J.P. Gowda, B.C.. Prasannakumara, N. A. Shah, S.U. Khan, J.D. Chung, Numerical study of bio-convection flow of magneto-cross nanofluid containing gyrotactic microorganisms with activation energy, Sci. Rep. 11 (2021) 16030.
[43] Y. Chu, M. Nazeer, M.I. Khan, F. Hussain H. Rafi, S. Qayyum, Z. Abdelmalek, Combined impacts of heat source/sink, radiative heat flux, temperature dependent thermal conductivity on forced convective Rabinowitsch fluid, Int. Commun. Heat Mass Transf. (2020), 105011.
[44] P.K. Pattnaik, M.M. Bhatti, S.R. Mishra, M.A. Abbas, O.A. Beg, Mixed Convective-Radiative Dissipative Magnetized Micropolar Nanofluid Flow over a Stretching Surface in Porous Media with Double Stratification and Chemical Reaction Effects: ADM-Padé Computation, J. Math. (2022), 9888379.
[45] M.K. Nayak, S. Shaw, M.I. Khan, Interfacial layer and shape effects of modified Hamilton's Crosser model in entropy optimized Darcy-Forchheimer flow, Alexandria Eng. J. 60 (4) (2021) 4067–4083.
[46] M.I. Khan, S. Qayyum, S. Shah, R.N. Kumar, R.J.P. Gowda, B.C.. Prasannakumara, S.Kadry Y.Chu, Marangoni convective flow of hybrid nanofluid (MnZnFe2O4-NiZnFe2O4-H2O) with Darcy Forchheimer medium, Ain Shams Eng. J. 12 (4) (2021) 3931–3938.
[47] T. Zhao, M.I. Khan, Y. Chu, Artificial neural networking (ANN) analysis for heat and entropy generation in flow of non-Newtonian fluid between two rotating disks, Math. Method Appl. Sci. (2021), https://doi.org/10.1002/mma.7310.
[48] M.M. Bhatti, H.F. Öztop, R. Ellahi, I.E. Sarris, M.H. Doranehgard, Insight into the investigation of diamond (C) and Silica (SiO2) nanoparticles suspended in water-based hybrid nanofluid with application in solar collector, J. Mol. Liq. 357 (2022), 119134.
[49] N.A. Shah, A.A. Zafar, S. Akhtar, General solution for MHD-free convection flow over a vertical plate with ramped wall temperature and chemical reaction, Arabian J. Math. 7 (2018) 49–60.
[50] N.A. Shah, A.U. Awan, R. Khan, Free convection Hartmann flow of a viscous fluid with damped thermal transport through a cylindrical tube, Chin. J. Phys. (2022), https://doi.org/10.1016/j.cjph.2021.09.019.
[51] Y.M. Chu, M.I.U. Rahman, M.I. Khan, Transportation of heat and mass transport in hydromagnetic stagnation point flow of Carreau nanomaterial: Dual simulations through Runge-Kutta Fehlberg technique, Int. Commun. Heat Mass Transf. 118 (2020), 104858.
[52] M. Nazeer, F. Hussain, M.I. Khan, et al., Theoretical study of MHD electro-osmotically flow of third-grade fluid in micro channel, Appl. Math. Comput. 420 (2022), 126868.
[53] W. Ibrahim, The effect of induced magnetic field and convective boundary condition on MHD stagnation point flow and heat transfer of upper-convected Maxwell fluid in the presence of nanoparticle past a stretching sheet, Prop. Power Res. 5 (2) (2016) 164–175.

[54] S. Naramgari, S. Chalavadi, A.I. Lare, Stagnation-point flow of Jeffrey nanofluid over a stretching surface with induced magnetic field and chemical reaction, Int. Eng. Res. Africa 20 (2016) 93–111.
[55] K. Naganthran, Md.F.Md. Basir, T. Thumma, E.O. Ege, R. Nazar, I. Tlili, Scaling group analysis of bioconvective micropolar fluid flow and heat transfer in a porous medium, J. Therm. Anal. Calorim. 143 (2021) 1943–1955.
[56] A.K. Verma, A.K. Gautam, K. Bhattacharyya, I. Pop, Entropy generation analysis in Falkner-Skan flow of Maxwell nanofluid in Darcian porous medium with temperature-dependent variable viscosity, Pramana J. Phys. 95 (2021) 69.
[57] S. Rajput, A.K. Verma, K. Bhattacharyya, A.J. Chamkha, Unsteady nonlinear mixed convective flow of nanofluid over a wedge: Buongiorno model, Waves Random Complex Media (2021), https://doi.org/10.1080/17455030.2021.1987586.
[58] A.K. Gautam, A.K. Verma, K. Bhattacharyya, S. Mukhopadhyay, A.J. Chamkha, Impacts of activation energy and binary chemical reaction on MHD flow of Williamson nanofluid in Darcy–Forchheimer porous medium: a case of expanding sheet of variable thickness, Waves Random Complex Media (2021), https://doi.org/10.1080/17455030.2021.1979274.
[59] A.K. Verma, K. Bhattacharyya, S. Rajput, M.S. Mandal, A.J. Chamkha, D. Yadav, Buoyancy driven non-Newtonian Prandtl-Eyring nanofluid flow in Darcy-Forchheimer porous medium over inclined non-linear expanding sheet with double stratification, Waves Random Complex Media (2022), https://doi.org/10.1080/17455030.2022.2062482.
[60] I.A. Hassanien, A.A. Abdullah, R.S.R. Gorla, Flow and heat transfer in a power-law fluid over a non-isothermal stretching sheet, Math. Comput. Model. 28 (9) (1998) 105–116.
[61] M.Z. Salleh, R. Nazar, Numerical solutions of the boundary layer flow and heat transfer over a stretching sheet with constant wall temperature and heat flux, Proc. Third Int. Conf. Math. Science-ICM 3 (2008) 1260–1267.
[62] F.Md. Ali, R. Nazar, N.Md. Arifin, I. Pop, MHD boundary layer flow and heat transfer over a stretching sheet with induced magnetic field, Heat Mass Transf. 47 (2011) 155–162.